

UCLA

UCLA Previously Published Works

Title

CH4 sources estimated from atmospheric observations of CH4 and its C-13/C-12 isotopic ratios: 2. Inverse modeling of CH4 fluxes from geographical regions

Permalink

<https://escholarship.org/uc/item/0vt1t4wd>

Journal

Global Biogeochemical Cycles, 18(4)

ISSN

0886-6236

Authors

Mikaloff Fletcher, S.E.

Tans, P P

Bruhwiller, L M

et al.

Publication Date

2004-10-01

Peer reviewed

CH₄ sources estimated from atmospheric observations of CH₄ and its ¹³C/¹²C isotopic ratios:

2. Inverse modeling of CH₄ fluxes from geographical regions

Sara E. Mikaloff Fletcher¹

Cooperative Institute for Research in Environmental Science (CIRES), University of Colorado, Boulder, Colorado, USA

Pieter P. Tans, Lori M. Bruhwiler, and John B. Miller

National Oceanic and Atmospheric Administration Climate Modeling Diagnostics Laboratory (NOAA CMDL), Boulder, Colorado, USA

Martin Heimann

Max-Planck-Institut Für Biogeochemie, Jena, Germany

Received 14 January 2004; revised 14 June 2004; accepted 24 July 2004; published XX Month 2004.

[1] We present a time-dependent inverse modeling approach to estimate the magnitude of CH₄ emissions and the average isotopic signature of the combined source processes from geographical regions based on the observed spatiotemporal distribution of CH₄ and ¹³C/¹²C isotopic ratios in CH₄. The inverse estimates of the isotopic signature of the sources are used to partition the regional source estimates into three groups of source processes based on their isotopic signatures. Compared with bottom-up estimates, the inverse estimates call for larger CH₄ fluxes in the tropics (266 ± 25 Tg CH₄/yr) and southern extratropics (98 ± 15 Tg CH₄/yr) and reduced fluxes in the northern extratropics (252 ± 18 Tg CH₄/yr). The observations of ¹³C/¹²C isotopic ratios in CH₄ indicate that the large a posteriori CH₄ source in the tropics and Southern Hemisphere is attributable to a combination both bacterial sources and biomass burning and support relatively low estimates of fossil CH₄ emissions. *INDEX TERMS*: 0315 Atmospheric Composition and Structure: Biosphere/atmosphere interactions; 0322 Atmospheric Composition and Structure: Constituent sources and sinks; 0368 Atmospheric Composition and Structure: Troposphere—constituent transport and chemistry; 1040 Geochemistry: Isotopic composition/chemistry; *KEYWORDS*: ¹³C/¹²C isotopic ratios, inverse modeling, methane sources

Citation: Mikaloff Fletcher, S. E., P. P. Tans, L. M. Bruhwiler, J. B. Miller, and M. Heimann (2004), CH₄ sources estimated from atmospheric observations of CH₄ and its ¹³C/¹²C isotopic ratios: 2. Inverse modeling of CH₄ fluxes from geographical regions, *Global Biogeochem. Cycles*, 18, GBXXXX, doi:10.1029/2004GB002224.

1. Introduction

[2] Atmospheric CH₄ plays a major role in Earth's radiative budget and atmospheric chemistry. CH₄ contributes about 20% of the total radiative forcing from long-lived greenhouse gases. CH₄ is also an important sink for OH radical, the major determinant of the oxidizing capacity of Earth's atmosphere, affects O₃ chemistry in the troposphere and the stratosphere, and leads to the production of stratospheric water vapor. The CH₄ mixing ratio in the atmosphere has increased by 150% since pre-industrial times, and based on the ice core record of atmospheric CH₄, current levels of CH₄ have not been exceeded for the last 420,000 years [Petit et al., 1999].

[3] A great deal of progress has been made toward estimating the sources and sinks of CH₄ through models of the source processes and combining local observations of CH₄ emissions or emission ratios with land use inventories, energy use or agricultural data, or other relevant statistical information [e.g., Matthews and Fung, 1987; Aselmann and Crutzen, 1989; Olivier et al., 1996; Levine et al., 2000; Kaplan, 2001]. However, owing to the large spatial and temporal variability of many of the source processes, these estimates are associated with a great deal of uncertainty. Forward model simulations which determine the atmospheric spatiotemporal distribution of CH₄ based on estimates of the sources and sinks have found that these bottom-up estimates lead to an overestimate of the inter-hemispheric gradient relative to the atmospheric observations [e.g., Fung et al., 1991; Hein et al., 1997; Houweling et al., 1999] (Figure 1), suggesting our process-level understanding of the CH₄ cycle is incomplete. In addition, bottom-up estimates often do not account for interannual

¹Now at the Department of Atmospheric and Oceanic Sciences, University of California, Los Angeles, California, USA.

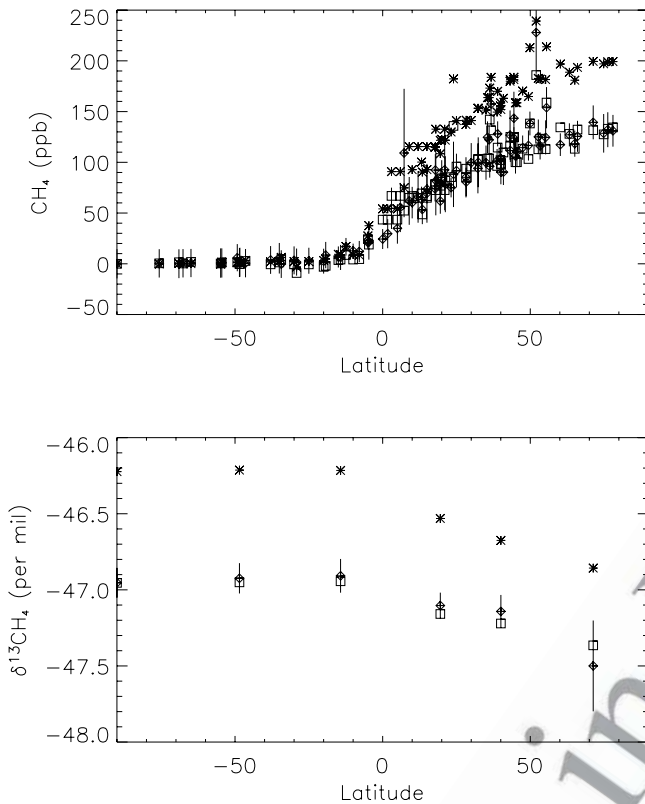


Figure 1. Latitudinal gradient of (top) CH_4 and (bottom) $\delta^{13}\text{CH}_4$ of the observations (diamonds), forward simulation based on the a priori estimates (asterisks), and forward simulation based on the a posteriori source estimates (squares). Error bars on the observations reflect the standard deviation of the individual observations from the annual mean.

variability of the CH_4 sources. Owing to the variability of the CH_4 growth rate [Dlugokencky et al., 2003, 2001], methods that elucidate the causes for interannual variability in the CH_4 cycle are highly desirable.

[4] Inverse modeling has also been used to optimize CH_4 fluxes based on observations of the atmospheric CH_4 mixing ratios and a model of atmospheric transport [e.g., Hein et al., 1997; Houweling et al., 1999; Bergamaschi et al., 2000; Chen, 2004]. Several inverse studies have used an estimate of the spatial footprint for each source process, the observations of CH_4 , and, in some cases, its $^{13}\text{C}/^{12}\text{C}$ isotopic ratios to estimate the global source strength of each source process [Hein et al., 1997; Bergamaschi et al., 2000; Mikaloff Fletcher et al., 2004]. This approach is subject to considerable uncertainty due to the inherent assumption that the a priori spatial pattern of the source processes is perfect and does not vary interannually. Inverse methods have been used to optimally estimate, within certain assumptions, the spatial pattern of the CH_4 flux required by the CH_4 observations [Houweling et al., 1999], without first partitioning the sources into source processes with their own spatial patterns. However, owing to the spatial overlap of the source processes, this approach does not

elucidate the underlying causes for changes in the CH_4 flux estimates.

[5] The observed $\text{CH}_4^{13}\text{C}/^{12}\text{C}$ isotopic ratio has also been used to constraint the CH_4 budget [e.g., Miller et al., 2002; Quay et al., 1999; Mikaloff Fletcher et al., 2004] due to the differing isotopic signatures of different source processes (Table 1). The $^{13}\text{C}/^{12}\text{C}$ isotopic ratio, R_{sample} , is often expressed as a deviation from an arbitrary standard, $R_{\text{reference}}$, in order to accentuate the very small changes in atmospheric $^{13}\text{C}/^{12}\text{C}$ due to the isotopic signatures of the sources.

$$\delta^{13}\text{C} = \left(\frac{R_{\text{sample}}}{R_{\text{reference}}} - 1 \right) \times 1000, \quad (1)$$

In this case, $R_{\text{reference}}$ is the Peedee Belemite carbonate standard [Craig, 1953]. Methane generated by bacteria in anaerobic environments including wetlands, rice paddies, and the digestive tracts of ruminant animals and termites is more depleted in ^{13}C than the background atmosphere, methane emitted from biomass burning is less depleted in ^{13}C than the background atmosphere, and CH_4 from fossil fuels such as coal and natural gas is relatively close to the atmospheric $\delta^{13}\text{C}$ signature. While landfill CH_4 emissions are generated by anaerobic bacteria, the isotopic signature of landfill CH_4 is less depleted in ^{13}C than the other bacterial sources due to partial oxidation of CH_4 within the landfill.

Table 1. A Priori CH_4 Source Estimates and the Mean $\delta^{13}\text{CH}_4$ Isotopic Signatures of the Sources and Sinks

	A Priori Estimates, Tg CH_4/yr	Mean Isotopic Signature	
<i>Sources</i>			
Bacterial sources			t1.1
Swamps	91 ^a	-58‰ ^b	t1.2
Bogs and tundra	54 ^a	-58‰ ^b	t1.3
Rice agriculture	60 ^c	-63‰ ^b	t1.4
Ruminant animals	93 ^c	-60‰ ^b	t1.5
Termites	20 ^d	-70‰ ^b	t1.6
Biomass burning	52 ^e	-25‰ ^b	t1.7
Fossil Fuels			t1.8
Coal	38 ^c	-37‰ ^b	t1.9
Natural gas and other industrial	57 ^c	-44‰ ^b	t1.10
Landfills	50 ^f	-55‰ ^b	t1.11
<i>Prescribed Sources and Sinks</i>			
Hydrates	10 ^g	-60‰ ^b	t1.12
Ocean	5 ^g	-60‰ ^b	t1.13
Tropospheric OH	507 ^h	5.4‰ ⁱ	t1.14
Stratospheric loss	40 ^j	12‰ ^k	t1.15
Soils	30 ^j	22‰ ^l	t1.16

^aLelieveld et al. [1998].

^bWhiticar [1993].

^cEDGAR emissions database [Olivier et al., 1996].

^dSanderson [1996].

^eLevine et al. [2000].

^fBingemer and Crutzen [1987].

^gCicerone and Oremland [1988].

^hOn the basis of Spivakovsky et al. [2000] OH fields and model CH_4 mixing ratios, tuned to IPCC [2001] total CH_4 loss.

ⁱCantrell et al. [1990].

^jIPCC [2001].

^kBrenninkmeijer et al. [1995], reflecting the total observed isotopic fractionation due to OH, O¹D, and Cl in the stratosphere.

^lTyler et al. [1994].

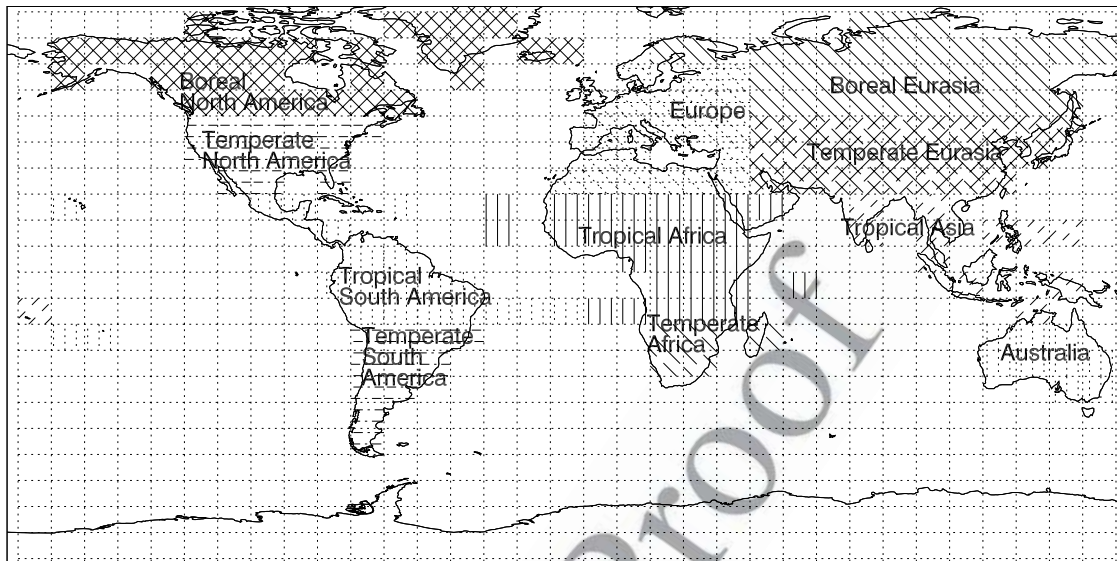


Figure 2. The eleven spatial land region definitions used in the inverse model.

[6] In this work, we demonstrate a novel approach to partition regional inverse estimates of CH_4 into three broad categories of source processes based on the atmospheric observations of $\delta^{13}\text{CH}_4$. We present time-dependent CH_4 fluxes from 11 geographical regions and inverse estimates of the $\delta^{13}\text{CH}_4$ isotopic signature from all source processes from three latitude bands for 1998–1999. The a posteriori isotopic signatures of the sources are used to determine the contributions of the bacterial, biomass burning and fossil fuel source processes to the a posteriori CH_4 fluxes and discuss the likely physical causes for differences between bottom-up source estimates and the inverse estimates. Changes in the annual mean fluxes for 1998–1999 are discussed in the context of the 1998 growth rate anomaly. Finally, the sensitivity of the inverse estimates is tested with respect to changes in several model parameters.

2. Methods

[7] The experimental design in this work is described in detail by Mikaloff Fletcher *et al.* [2004]. Here we provide a brief overview of the model setup, then focus on the differences between these two studies.

[8] The model transport is represented by the coarse grid version of Tracer Model 3 (TM3) [Heimann and Körner, 2003] with a resolution of 7.8° latitude by 10° longitude by nine vertical levels. TM3 was driven by The National Centers for Weather Prediction/National Center for Atmospheric Research (NCEP/NCAR) wind fields corresponding to the year being modeled. The model was initialized using three-dimensional CH_4 and $\delta^{13}\text{CH}_4$ fields from the final time step of a “test” inversion which was initialized using observed hemispheric mean values [Miller *et al.*, 2002]. The first 3 months of the final inverse results were excluded to minimize inaccuracies due to initial conditions. The CH_4 sinks were prescribed as described by Mikaloff Fletcher *et al.* [2004].

[9] Mikaloff Fletcher *et al.* [2004] estimated the global total source strength for each source process. This allows

the isotopic fractionation of each source to be prescribed in order to use the isotopic ratios measured at each observing station as additional constraints on the methane flux estimates. In this study, the world is divided into 11 geographical regions (Figure 2), and CH_4 flux is estimated for each spatial region based on the GLOBALVIEW- CH_4 [National Oceanic and Atmospheric Administration (NOAA), 2001] data set and a priori estimates of the sources (Table 1). Since the emissions within a spatial region are typically due to many source processes whose relative contributions are poorly known, the isotopic signatures of the net source from each model region is calculated using the inverse model constrained by observations of the isotopic signature at six observing stations from the NOAA/CMDL network shown in Table 2 [Miller *et al.*, 2002] and a priori estimates based on the flux estimates and isotopic signatures in Table 1. These isotopic signatures are then used as an additional constraint on the total CH_4 flux and to partition the regional fluxes between source processes. Only six observing stations with measurements of $\delta^{13}\text{CH}_4$ were included in this work, so the inverse model will not be able to constrain all 11 model regions for $\delta^{13}\text{CH}_4$. Thus, for the inversion for

Table 2. NOAA/CMDL Cooperative Air Sampling Network Sites With $\delta^{13}\text{CH}_4$ Observations

Name	Site Code	Location	Elevation, m	
Barrow, Alaska, USA	BRW	$71^\circ 19' \text{N}$ $156^\circ 36' \text{W}$	11	t2.3
Niwot Ridge, Colorado, USA	NWR	$40^\circ 03' \text{N}$ $105^\circ 35' \text{W}$	3475	t2.4
Mauna Loa, Hawaii, USA	MLO	$19^\circ 32' \text{N}$ $155^\circ 35' \text{W}$	3397	t2.5
Cape Matatula, American Samoa	SMO	$14^\circ 15' \text{N}$ $170^\circ 34' \text{W}$	42	t2.6
Cape Grim, Tasmania	CGO	$40^\circ 41' \text{S}$ $144^\circ 41' \text{E}$	94	t2.7
South Pole, Antarctica	SPO	$89^\circ 59' \text{S}$ $24^\circ 48' \text{W}$	2810	t2.8

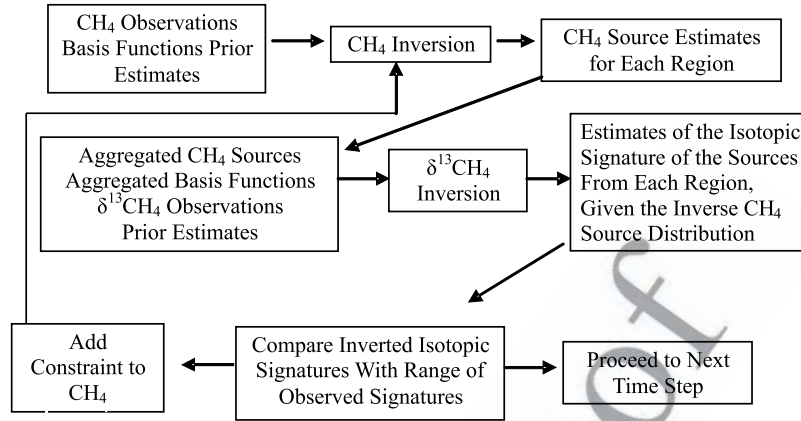


Figure 3. Schematic description of the iterative process used to estimate CH_4 sources and $\delta^{13}\text{CH}_4$.

170 the isotopic signatures, these regions are aggregated to three
171 latitude bands: north of 23.5°N , 23.5°N to 15.7°S , and south
172 of 15.7°S .

173 [10] Although there are long-term observational records
174 of $\delta^{13}\text{CH}_4$ at a number of observing stations [e.g., *Lowe et al.*,
175 *1994*; *Quay et al.*, *1999*; *Bergamaschi et al.*, *2000*], only
176 the observations from the NOAA/CMDL network were
177 included in the inverse model. *Miller et al.* [2002]
178 demonstrated that there may be offsets between laboratories
179 of about 0.1‰ , which could lead to significant biases in the
180 inverse model. This highlights the need for $\delta^{13}\text{CH}_4$
181 measurement intercomparisons.

182 [11] Like *Mikaloff Fletcher et al.* [2004], monthly fluxes
183 for 1998–2000 were estimated using a time-dependent
184 mass balance inversion [*Bruhwiller et al.*, *2000*]. The
185 difference between the observed mixing ratio of a trace
186 gas at the j th station, y_j^{obs} , and the model simulated mixing
187 ratio in the absence of sources, y_j , is treated as the sum over
188 nreg discrete model regions of the source strengths, x_i ,
189 multiplied by basis functions, $H_{i,j}$, which represent the
190 atmospheric response at the j th station to an arbitrary unit
191 flux from the i th region.

$$y_j^{\text{obs}} - y_j = \sum_{i=1, \text{nreg}} \mathbf{H}_{i,j} x_i. \quad (2)$$

193 The modeled mixing ratio, y_j^{obs} , is calculated by applying
194 the transport model to the three-dimensional tracer field
195 from the previous month. The basis function for a given
196 region and a given month is simulated by emitting a steady
197 flux from the region, distributed spatially within the region
198 according to an a priori estimate of the sources, and
199 allowing the transport model to act on these emissions.
200 Then, the modeled three-dimensional mixing ratio field is
201 sampled at the station locations at the end of the month.

202 [12] In order to estimate the isotopic signature of the
203 sources, equation (2) can be rewritten in terms of the mixing
204 ratio ^{13}C and the $^{13}\text{C}/^{12}\text{C}$ isotopic ratio of the sources from
205 each region, R_i , as follows:

$$y_{j13c}^{\text{obs}} - y_{j13c} = \sum_{i=1, \text{nreg}} H_{i,j} x_i R_i. \quad (3)$$

By dividing equation (3) by $R_{\text{reference}}$, then subtracting
equation (2), the following expression can be written

$$\frac{y_{j13c}^{\text{obs}} - y_{j13c}}{R_{\text{reference}}} - (y_j^{\text{obs}} - y_j) = \sum_{\text{nsrc}} H_{i,j} x_i \left(\frac{R_i}{R_{\text{reference}}} - 1 \right). \quad (4)$$

Dividing equation (4) by equation (2) and multiplying by
1000, this equation begins to take on the form of δ units
(equation (1)), which are needed to emphasize the small
differences in $^{13}\text{C}/^{12}\text{C}$ ratios caused by the isotopic
signatures of the sources.

$$\left(\frac{y_{j13c}^{\text{obs}} - y_{j13c}}{(y_j^{\text{obs}} - y_j) R_{\text{std}}} - 1 \right) \times 1000 = \frac{\sum_{\text{nsrc}} H_{i,j} x_i \delta_i}{\sum_{\text{nsrc}} H_{i,j} x_i}. \quad (5)$$

The left-hand side of equation (5) is the “effective” δ value
of the net difference between observed and simulated
mixing ratios, which is defined here as δ_{diff}

$$\delta_{\text{diff}} = \left[\frac{y_{j13c}^{\text{obs}} - y_{j13c}}{(y_j^{\text{obs}} - y_j) R_{\text{std}}} - 1 \right] \times 1000. \quad (6)$$

For a small fraction of data points, the difference $y_{j13c}^{\text{obs}} - y_{j13c}$
is very close to zero, which leads to spurious values of
 δ_{diff} . These data are excluded from the inversion. In the
inverse model, this difference represents the total signal of
the sources at the station over a given month (equation (3));
therefore, these data points are not likely to provide a strong
constraint to the inverse model.

[13] Note that equation (5) contains nonlinearity, as it is
dependent on x_i and δ , both of which are variable in the
inverse model. An iterative approach is used to deal with
this problem, shown schematically in Figure 3. First,
equation (2) is solved for the CH_4 sources. Then, the basis
functions and sources are aggregated to the larger $\delta^{13}\text{CH}_4$
source regions, and equation (5) is solved for the isotopic
signature of the sources holding the sources fixed. The
calculated isotopic signatures from each source region can
be used both qualitatively and quantitatively as an
interpretive tool to partition the fluxes within spatial regions

t3.1 **Table 3.** Summary of the Inversion Scenarios Implemented to Compare Prior Estimates With Inverse Results and Test the Sensitivity of the Inverse Results to Various Sources of Error

t3.2	Scenario	Description	Additional Details
t3.3	S0	a priori source estimates	forward simulation of prior source estimates shown in Table 1.
t3.4	S1	a posteriori estimates, including observations of $\delta^{13}\text{C}$	inverse source estimates
t3.5	S2	sensitivity to OH kinetic isotope effect	S1 with the <i>Saueressig et al.</i> [2001] measurement of the KIE for OH
t3.6	S3	sensitivity to OH fields- Upper limit	S1 with OH increased by 15% to the upper end of the uncertainty estimate of <i>Spivakovsky et al.</i> [2000]
t3.7	S4	sensitivity to OH fields- Lower limit	S1 with OH decreased 15% to the lower end of the uncertainty estimate of <i>Spivakovsky et al.</i> [2000]
t3.8	S5	sensitivity to initial conditions	S1 initialized to the observed hemispheric mean CH_4 and $\delta^{13}\text{C}$ for 1998 [<i>Miller et al.</i> , 2002]

238 between source processes. Finally, the inverse isotopic
239 signatures are compared to the range of observed isotopic
240 signatures of the source processes (Table 1) and in some
241 cases used to constrain the CH_4 estimates.

242 [14] In the absence of error, the a posteriori isotopic
243 signature for a given latitude band could only match the
244 high or low end of this range of isotopic signatures if the
245 CH_4 flux from the latitude band were composed almost
246 entirely of either biomass burning or bacterial sources. At a
247 few model time steps, the estimated isotopic signature
248 exceeds the range of isotopic signatures of the source
249 processes. There is considerable uncertainty associated with
250 the isotopic signatures of the source processes. However, an
251 a posteriori isotopic signature of this magnitude would
252 require both a significant excursion from the observed
253 isotopic signature of the source processes and the unlikely
254 source scenario mentioned above. Therefore it seems rea-
255 sonable to assume in these cases that there may be an error
256 in the inverse estimate of CH_4 .

257 [15] When the a posteriori isotopic signatures are greater
258 than -25% or less than -65% , a feedback mechanism is
259 activated to constrain the CH_4 flux estimates using the
260 isotope data. This constraint is formulated by re-arranging
261 equation (5) and replacing the a posteriori estimate of δ_i for
262 the regions with spurious isotopic signature estimates with
263 either the minimum or maximum in the range of signatures
264 from the source processes, $\delta_{\min/\max}$.

$$\delta_{\text{diff}} \sum_{\text{nsrc}} H_{ij} x_i = \sum_{\text{nsrc}} H_{ij} x_i \delta_{\min/\max}. \quad (7)$$

266 [16] The total effect of the sources, $\sum_{\text{nsrc}} H_{ij} x_i$, is treated as a
267 constant, since this quantity is equal to the difference $y_j^{\text{obs}} -$
268 y_j . This is repeated iteratively until the criteria of a match to
269 the station observations of CH_4 , $\delta^{13}\text{C}$, and the range of
270 reasonable isotopic signatures are all matched. While we
271 correct the CH_4 flux estimates with the isotopic data in these
272 cases where the presence of an error is clear, one important
273 weakness of this technique is that any error associated with
274 the CH_4 source estimates is propagated to the $\delta^{13}\text{C}$
275 estimates.

276 [17] The a priori CH_4 flux estimates and spatial patterns
277 for these land regions were calculated by distributing the a
278 priori source process estimates (Table 1) spatially according
279 the NASA Goddard Institute for Space Studies (GISS) flux
280 maps [*Fung et al.*, 1991], and the uncertainties assigned to
281 the prior estimates are based on the range of estimates given
282 by the *IPCC* [2001], as per *Mikaloff Fletcher et al.* [2004].

283 Similarly, the a priori $\delta^{13}\text{C}$ isotopic signatures are based on
284 a flux-weighted average of the isotopic signatures shown in
285 Table 1 for each region. An uncertainty of 0.15‰ was
286 assigned to the prior estimates. This value was selected
287 based on equilibrium estimates of how much relatively large
288 changes in the fluxes or the isotopic signatures of the
289 sources might change the a priori isotopic signature on large
290 spatial scales. For example, a shift of 100 Tg of CH_4 from
291 wetlands to biomass burning would result in a change in the
292 global isotopic signature of about 0.15‰ based on a global
293 total source of 550 Tg CH_4/yr , and a change in the global
294 wetland isotopic signature of 0.13‰ based on the source
295 estimates of *Mikaloff Fletcher et al.* [2004]. The relatively
296 large uncertainty estimates associated with the priors were
297 chosen to allow a strongly data-driven inversion. The
298 uncertainties assigned to the CH_4 observations were based
299 on the mean standard deviation of the observations from the
300 smoothed curve, as described by *Mikaloff Fletcher et al.*
301 [2004]. The uncertainty associated with the calculated δ_{diff}
302 σ_{diff} is calculated using mean values of the differences y_j^{obs}
303 $- y_j$ and $y_{j_{13\text{C}}}^{\text{obs}} - y_{j_{13\text{C}}}$ and the uncertainties for these two
304 differences, σ_{CH_4} and $\sigma_{\text{C}13}$.

$$\sigma_{\text{diff}} = \sqrt{\left(\frac{\sigma_{\text{CH}_4} (y_{j_{13\text{C}}}^{\text{obs}} - y_{j_{13\text{C}}})}{R_{\text{std}}}\right)^2 + \left(\frac{\sigma_{\text{CH}_4}}{(y_j^{\text{obs}} - y_j) R_{\text{std}}}\right)^2}. \quad (8)$$

306 Like σ_{CH_4} , $\sigma_{\text{C}13}$ is calculated based on the mean standard
307 deviation of the observations from the smoothed curve.
308 Finally, for cases in which the isotopes are used to constrain
309 the CH_4 flux estimates using equation (6), σ_{const} , the
310 uncertainty associated with this constraint is represented by

$$\sigma_{\text{const}} = \sqrt{(\sigma_{\Sigma H_x} \times \delta_{\text{diff}})^2 + \left(\sigma_{\text{diff}} \sum_{\text{nsrc}} H_{ij} x_i\right)^2}, \quad (9)$$

312 where the uncertainty associated with the sum of the
313 methane sources multiplied by the basis functions, $\sigma_{\Sigma H_x}$ was
314 taken to be 20% of the value of the total.

315 [18] In section 7, the sensitivity of the inverse technique
316 to several potential sources of error is tested using the
317 scenarios summarized in Table 3.

3. Inverse CH_4 Estimates

318 [19] Overall, the a posteriori sources in the Northern
319 Hemisphere (NH) are decreased relative to a priori esti-
320

t4.1 **Table 4.** Time-Averaged CH₄ Source Estimates for the A Priori Fluxes (S0), and the A Posteriori Estimates for Several Inverse Scenarios Described in Table 1^a

t4.2	Model Region	S0	S1	S2	S3	S4	S5
t4.3	Boreal North America	21 ± 16	16 ± 4	13 ± 5	13 ± 5	15 ± 4	21 ± 4
t4.4	Boreal Eurasia	43 ± 28	15 ± 8	23 ± 8	24 ± 9	15 ± 8	9 ± 8
t4.5	Temperate North America	58 ± 13	54 ± 8	56 ± 9	59 ± 9	45 ± 8	46 ± 8
t4.6	Europe	69 ± 15	69 ± 8	64 ± 8	66 ± 8	65 ± 8	72 ± 8
t4.7	Temperate Eurasia	98 ± 42	98 ± 11	103 ± 11	106 ± 11	86 ± 11	88 ± 11
t4.8	Tropical South America	53 ± 25	73 ± 16	77 ± 17	87 ± 17	44 ± 15	62 ± 15
t4.9	Northern Africa	47 ± 21	80 ± 17	73 ± 17	79 ± 17	63 ± 17	86 ± 17
t4.10	Tropical Asia	76 ± 38	113 ± 10	112 ± 10	119 ± 10	93 ± 9	114 ± 10
t4.11	Southern Africa	9 ± 3	10 ± 2	10 ± 2	10 ± 2	9 ± 2	10 ± 2
t4.12	Temperate South America	36 ± 20	71 ± 14	73 ± 15	81 ± 15	50 ± 13	70 ± 13
t4.13	Australia	13 ± 4	17 ± 4	19 ± 4	20 ± 4	15 ± 4	16 ± 3
t4.14	Global	523 ± 78	618 ± 28	624 ± 29	662 ± 30	498 ± 28	592 ± 28

t4.15 ^aNote that the relatively small ocean sources and all of the CH₄ sinks have been prescribed.

321 mates, while sources in the Southern Hemisphere (SH) are
 322 increased relative to the prior estimates (Table 4, Figure 4),
 323 a robust result that is in general agreement with the forward
 324 results (Figure 1) and previous inverse studies [i.e., *Mikaloff*
 325 *Fletcher et al.*, 2004; *Houweling et al.*, 1999; *Hein et al.*,
 326 1997; *Chen*, 2004]. The bulk of this reduction occurs in
 327 boreal Eurasia, with a smaller reduction in boreal North
 328 America. These high northern latitude regions are well
 329 sampled by the observing network and well constrained by
 330 the CH₄ observations, given the a priori detailed spatial
 331 patterns. The observations also call for smaller emissions
 332 from temperate North America than the prior estimates, but
 333 this difference is much smaller than the error limits
 334 estimated by the inverse model. The inverse model
 335 estimates the largest increases over the a priori estimates
 336 in the tropical regions of South America, Africa, and Asia.
 337 There are also significant increases in emissions from
 338 temperate South America. This region coincides with a
 339 major region of wetlands in the SH [*Kaplan*, 2001; *Walter*,
 340 1998]. However, owing to the paucity of CH₄ observations
 341 that constrain these regions, the partitioning between
 342 temperate South America, Southern Africa, and Australia
 343 may not be robustly driven by the observations. In addition,
 344 the observational constraints lead to reductions in the
 345 uncertainties associated with the a priori estimates, especially
 346 for regions in the NH.

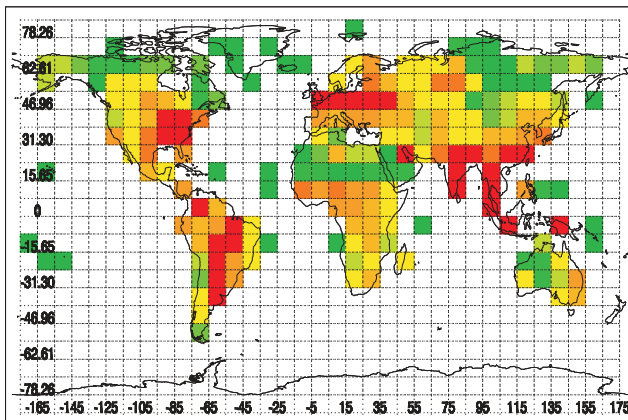
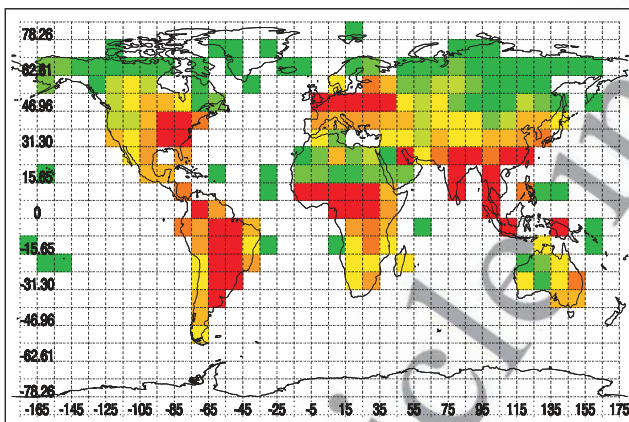
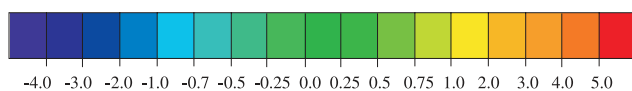
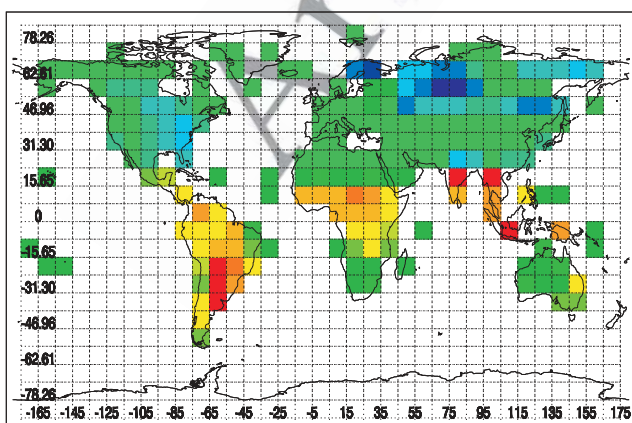
347 [20] The two-dimensional spatial distribution of CH₄ flux
 348 that would result from these regional source estimates has
 349 been illustrated by distributing the regional fluxes according
 350 to the spatial patterns used for the basis functions (Figure 3).
 351 As discussed above, the overall interhemispheric gradient
 352 and many continental scale features are similar between this
 353 approach and a source process inversion [*Mikaloff Fletcher*
 354 *et al.*, 2004]. For example, both approaches call for large
 355 flux increases over tropical South America and Central
 356 Africa compared to the a priori estimates and large
 357 decreases in North America and Europe. This shows that
 358 these broad results are robust with respect to different
 359 definitions of the model regions and different approaches to
 360 the application of the isotopes to constrain the CH₄ flux.
 361 However, the regional details are distinctly different. The
 362 source process approach attributed much of the decrease in
 363 NH sources to fossil fuels and landfills; therefore the
 364 greatest a posteriori decreases occur in the industrial regions

of the United States and Europe. Conversely, the regional
 inversion assigns the largest decreases to high northern
 latitude regions, especially boreal Eurasia which would be
 more likely to be associated with emissions from boreal
 wetlands. In section 4, the ¹³C isotopic signatures will be
 used to determine which source process is most consistent
 with the observations.

[21] It is worthy of note that this inversion uses large
 spatial regions, and the total flux from a region can only
 shift according to the assumed spatial pattern, which is
 based on a priori source estimates. One approach that has
 been used to deal with artifacts in atmospheric inverse
 models caused by the use of large model regions is to treat
 each model grid cell as an individual model region [i.e.,
Kaminski et al., 1999; *Houweling et al.*, 1999]. This
 approach eliminates the need for “hard constraints,” or
 features of the trace gas flux that cannot be varied by the
 inverse model, such as the spatial pattern of the model
 regions. However, the trade-off associated with the use of a
 very large number of model regions is that the problem is
 very poorly constrained by the observations, and in the
 absence of good observational constraints to the inverse
 problem the solution can be heavily biased by the a priori
 estimates. With planned future expansions to the observing
 network and satellite observations, the use of very small
 model regions is a logical next step for inverse models;
 however, on the basis of the currently available observa-
 tional network, the use of large model regions was chosen
 for this research to provide strongly data-driven inverse
 estimates.

4. Inverse δ¹³C Estimates

[22] Since observations of δ¹³CH₄ are only available for
 six observing stations, the 11 model regions are aggregated
 to three latitude bands, and the inverse model is used to
 estimate the net δ¹³CH₄ isotopic signature from all of the
 source processes occurring within a model region. This
 isotopic signature is then used to interpret the likely reasons
 for important differences between the a priori estimates and
 the a posteriori estimates both qualitatively and quantita-
 tively (Table 5). The largest change in the isotopic signature
 of the sources occurs in the southern extratropical region,
 where the a posteriori isotopic signature of the sources is

Total *A Priori* FluxTotal *A Posteriori* FluxDifference Between *A Posteriori* and *A Priori*Methane Flux (Tg CH₄/grid box)

less depleted in ¹³C than the a priori estimate. Since the total 407
source is increased in this region, the heavier isotopic 408
signature suggests that the sources that are underestimated 409
in the a priori estimates are those that have heavier isotopic 410
signatures, such as biomass burning, although this difference 411
is not large relative to the a posteriori flux increase, so 412
bacterial sources are likely to be underestimated as well. 413

[23] In the tropics, the estimated isotopic signature is very 414
close to the a priori estimate. It could be argued that poor 415
overall sampling in the tropics may mean that this region is 416
so poorly constrained by the observational data that no new 417
information has been added by the inversion. However, in a 418
regime with only three model regions, if two are reasonably 419
well constrained by the observations, the third is then 420
constrained by mass balance. The CH₄ inversion calls for 421
a large increase in the net source for this region, and the 422
similar inverse isotopic signature implies that a combination 423
of sources that are much more depleted in ¹³C relative to the 424
atmosphere and those that are enriched relative to the 425
atmosphere must be increased relative to the a priori 426
estimates to maintain the isotope balance. The two isotopi- 427
cally depleted sources that play a major role in the tropics 428
are swamps and ruminant animals. Of these two, the 429
ruminant animal source is relatively well known based on 430
bottom-up inventory techniques, but the swamp source is 431
not, making it the most likely source for a large increase. 432
Biomass burning is very isotopically enriched relative to the 433
background atmosphere, so the isotopic signature of the 434
tropical sources implies large increases in the swamp and 435
biomass burning sources compared to the a priori estimates. 436
This result from the regional inversion is in general agree- 437
ment with the source-process inversion, which called for 438
very high CH₄ fluxes from swamps and biomass burning 439
which both have large spatial footprints in the tropics 440
[Mikaloff Fletcher *et al.*, 2004]. 441

[24] Finally, in the northern extratropics, the inverse 442
model calls for a similar isotopic signature to the a priori 443
estimates, while the CH₄ inversion calls for a decreased 444
flux. Since the total flux is decreased and the isotopic 445
signature remains similar, either the isotopically heavy 446
and isotopically light sources must both be decreased or 447
sources with a weak isotopic signature relative to the 448
background atmosphere, such as fossil fuels, must be 449
decreased the most. This is a reasonable result for this 450
region since the bulk of the fossil fuel source is emitted in 451
the northern extratropical region. 452

[25] While this qualitative discussion is useful, a more 453
rigorous source partitioning is highly desirable in order to 454
further understanding of the a posteriori CH₄ fluxes. To this 455
end, the CH₄ sources have been grouped into three major 456
categories based on their isotopic signatures: fossil fuels and 457

Figure 4. Global distribution of CH₄ flux in Tg CH₄ grid 458
cell⁻¹ yr⁻¹ averaged over the 1998–1999 inversion time 459
period for (top) a priori estimates and (middle) a posteriori 460
estimates, and (bottom) the difference between the a 461
posteriori estimate and the a priori estimates. This source 462
map was created by distributing the flux estimates from the 463
11 source regions according to the spatial patterns used to 464
create the basis functions. 465

t5.1 **Table 5.** Time-Averaged Total ^{13}C Isotopic Signature and CH_4 Flux From Three Latitude Bands (North of 23.5°N , 23.5°N to 15.7°S , and South of 15.7°S) Partitioned Into Bacterial and Biomass Burning Sources^a

t5.2	Model Region	S0	S1	S2	S3	S4	S5
t5.3		<i>Northern Extratropics</i>					
t5.4	^{13}C isotopic signature	-53.3‰	-53.5‰	-53.2‰	-52.6‰	-54.1‰	-53.0‰
t5.5	Bacterial sources, Tg CH_4/yr	159	124–159	128–163	133–168	107–134	114–149
t5.6	Biomass burning, Tg CH_4/yr	2	-33–-5	-31–-3	-27–1	-41–-13	-34–-6
t5.8		<i>Tropics</i>					
t5.9	^{13}C isotopic signature	-50.3‰	-50.4‰	-48.5‰	-50.1‰	-49.9‰	-51.7‰
t5.10	Bacterial sources, Tg CH_4/yr	122	184–187	164–167	204–207	131–134	191–194
t5.11	Biomass burning, Tg CH_4/yr	48	65–68	81–84	83–85	54–57	58–61
t5.13		<i>Southern Extratropics</i>					
t5.14	^{13}C isotopic signature	-55.8‰	-53.9‰	-51.5‰	-54‰	-53.5‰	-54.9‰
t5.15	Bacterial sources, Tg CH_4/yr	44	76–78	73–75	94–97	56–58	76–79
t5.16	Biomass burning, Tg CH_4/yr	3	13–15	20–23	14–16	9–11	11–13

^aThe isotopic signatures represent the net isotopic signatures from all source processes and were estimated for the scenarios described in Table 2. The total CH_4 source for each latitude band, aggregated from the regional estimates in Table 3, was partitioned into bacterial and biomass burning sources using the estimated net isotopic signature of the total flux, the observed isotopic signatures for each source process, and upper and lower limits of the fossil fuel estimates. Note that the ranges shown in the a posteriori estimates only reflect the

t5.17 upper and lower bounds of the fossil fuel range and do not include uncertainty in the inverse estimates.

458 landfills, biomass burning, and bacterial sources, which
 459 include wetlands, ruminant animals, rice paddies, and
 460 termites. The mean isotopic signature for each of these
 461 source processes was calculated for each latitude band
 462 based on a priori estimates. Using mass balance, two
 463 equations can be written in terms of three unknowns for
 464 each latitude band,

$$S_{\text{tot}} = S_{\text{ba}} + S_{\text{bb}} + S_{\text{ff}} \quad (10)$$

$$\delta_{\text{tot}} S_{\text{tot}} = \delta_{\text{ba}} S_{\text{ba}} + \delta_{\text{bb}} S_{\text{bb}} + \delta_{\text{ff}} S_{\text{ff}} \quad (11)$$

468 where S denotes the source strength, δ denotes the isotopic
 469 signature, and the subscripts ba, bb, ff, and tot refer to
 470 bacterial sources, biomass burning sources, fossil sources,
 471 and the total source, respectively. Using the inverse model,
 472 the total source and isotopic signatures for each region, S_{tot}
 473 and δ_{tot} , have been determined. If one of the source
 474 processes could be prescribed, then the other two could be
 475 calculated from these equations. The most well known of
 476 these three broad categories is the fossil fuel group;
 477 therefore, the upper and lower bounds of the IPCC [2001]
 478 range of estimates for the fossil fuels were applied to these
 479 equations, resulting in the high and low estimates of
 480 bacterial and biomass burning sources (Table 5). Note that
 481 this range does not include uncertainty associated with the
 482 inverse estimates or the isotopic signatures of the sources,
 483 although the sensitivity of this quantity to changes in the
 484 inverse estimates will be explored in the next section.

485 [26] In the northern extratropics, the bacterial sources are
 486 reduced by this partitioning technique relative to the a priori
 487 estimates. Interestingly, the source partitioning finds a
 488 negative estimate for biomass burning sources, which is
 489 clearly a nonphysical result. This suggests that the fossil
 490 fuel estimates may be too high, in general agreement with
 491 the process-inversion approach, the prescribed sinks may be
 492 too low, or the total flux estimates may be too high in this
 493 region. The fossil fuel estimates used in this study may be

overestimated for Europe; since the spatial distribution of
 CH_4 used here predates the collapse of the Soviet Union, the
 spatial distribution of fossil fuels may be overestimated at
 high northern latitudes. *Dlugokencky et al.* [2003] attributed
 the decline in the CH_4 growth rate in the early 1990s to the
 collapse of the Soviet Union which caused changes in the
 interhemispheric gradient of the observed atmospheric CH_4 .

[27] In comparison to the northern extratropics, the tropics
 and southern extratropics have a small range of estimates
 due to the relatively small fossil emissions in these areas.
 Large increases have been estimated for both bacterial and
 biomass burning sources for these regions. Since ruminant
 animals are the most well known source and rice cultivation
 has a more limited spatial extent, wetlands are likely to
 contribute to a large portion of this bacterial increase. A
 high wetland source is in general agreement with recent
 source-process inverse studies [e.g., *Mikaloff Fletcher et al.*,
 2004; *Hein et al.*, 1997]. In addition, some recent wetland
 models have estimated a large spatial extent of wetlands
 [Kaplan, 2001] and very high CH_4 fluxes [Walter, 1998]
 compared with wetland inventory approaches. *Chen* [2004]
 found emissions from biomass burning and bacterial
 sources with strong spatial footprints in the tropics that
 were close to the high end of the range of bottom-up source
 estimates, but are still lower than the inverse estimates
 presented here.

5. Interannual Variability

[28] One of the key advantages of inverse modeling is the
 ability to diagnose observed anomalies in the atmospheric
 mixing ratio of a trace gas when clear, quantitative process-
 level observations of the source phenomenon responsible
 are not available. The annual means for 1998 and 1999 can
 be used to attempt to attribute the 1998 CH_4 growth rate
 anomaly [*Dlugokencky et al.*, 2001] to a region or source
 process. Since the model requires 3 months of spin-up time,
 and the $\delta^{13}\text{C}$ observations did not begin until 1998, the
 inverse estimates for 1998 are only for April–December.

t6.1 **Table 6.** Mean A Priori and Inverse Estimates of CH₄ Flux From the 11 Inverse Model Regions for April to December 1998 and All of 1999^a

t6.2 Model Region	A priori Estimates April–Dec. Mean, Tg CH ₄ /yr	A Posteriori (S1) 1998 April–Dec. Mean, Tg CH ₄ /yr	A Priori Estimates Annual Mean, Tg CH ₄ /yr	A Posteriori (S1) 1999 Annual Mean, Tg CH ₄ /yr
t6.3 Boreal North America	24 ± 16	23 ± 6	19 ± 16	12 ± 4
t6.4 Boreal Eurasia	48 ± 28	26 ± 9	39 ± 28	8 ± 7
t6.5 Temperate North America	58 ± 13	62 ± 9	58 ± 13	49 ± 8
t6.6 Europe	71 ± 15	60 ± 8	68 ± 15	76 ± 8
t6.7 Temperate Eurasia	103 ± 42	112 ± 11	94 ± 42	87 ± 10
t6.8 Tropical South America	53 ± 25	83 ± 18	53 ± 25	67 ± 15
t6.9 Northern Africa	47 ± 21	80 ± 16	48 ± 21	80 ± 17
t6.10 Tropical Asia	76 ± 38	117 ± 10	76 ± 38	110 ± 9
t6.11 Southern Africa	8 ± 3	9 ± 2	9 ± 3	10 ± 3
t6.12 Temperate South America	36 ± 20	64 ± 14	37 ± 20	77 ± 14
t6.13 Australia	13 ± 4	19 ± 4	13 ± 4	16 ± 4
t6.14 Global	537 ± 78	651 ± 29	515 ± 78	584 ± 28

t6.15 ^aNote that the a priori source estimates do not include interannual variability. The differing a priori sources from 1998 to 1999 reflect the seasonality of the sources since the two time-averaged values include different months.

531 The differences in the 1998 and 1999 a priori estimates
532 (Tables 6 and 7) reflect this seasonal bias, and there is no
533 interannual variability in the a priori estimates.

534 [29] 1998 was characterized by a transition from a very
535 strong El Niño, lasting until early May, to a La Niña,
536 beginning in July [Bell *et al.*, 1999]. Model simulations of
537 atmospheric CH₄ mixing ratios have shown that meteorol-
538 ogy can have an important effect on interannual variations
539 in atmospheric CH₄ [Warwick *et al.*, 2002]. However,
540 interannual variability due to changes in meteorology is
541 accounted for because the model is driven by assimilated
542 meteorological fields corresponding to the model year rather
543 than repeating a single year of meteorology.

544 [30] The bulk of the wetlands in the northern extratropical
545 latitude band occur in the boreal North America and boreal
546 Eurasia model regions. The inverse emissions estimates are
547 larger for these regions in 1998 than 1999 (Table 6). In
548 addition, the estimated isotopic signature is much more
549 depleted in ¹³C in 1998 than 1999 (Table 7), leading to a
550 large decrease in the calculated bacterial sources from 1998

to 1999. Since ruminant animal sources do not vary greatly
551 on interannual timescales and termites and rice paddies are
552 only minor contributors to the budget in these regions, this
553 change is attributable to wetlands in general agreement with
554 the conclusions of Dlugokencky *et al.* [2001] and the source
555 process inversion [Mikaloff Fletcher *et al.*, 2004]. The year
556 1998 was marked by elevated temperatures in boreal North
557 America and Eurasia from June to August [Bell *et al.*, 1999]
558 and elevated precipitation in some high northern latitude
559 regions from April to September [Curtis *et al.*, 2001], which
560 could explain elevated wetland emissions from high-latitude
561 wetlands [Dlugokencky *et al.*, 2001]. Although there is a
562 large range in the source partitioning for this region due to
563 the uncertainty in the fossil sources, since none of the fossil
564 sources is known to have such large variability on these
565 timescales, the interannual change is expected to be robust.

[31] In the tropics and southern extratropics, the 1998–
567 1999 variability in the a posteriori CH₄ flux and δ¹³C
568 isotopic signature is much smaller than in the northern
569 extratropics. Owing to the relatively small variability and
570

t7.1 **Table 7.** Mean A Priori and Inverse Estimates of the CH₄ Sources for April to December 1998 and All of 1999 Partitioned Using the Isotopic Signatures of the Sources and the Upper and Lower Bounds of Estimated Fossil Fuel Emissions^a

t7.2 Model Region	A Priori Estimates April–Dec. Mean, Tg CH ₄ /yr	A Posteriori (S1) 1998 April–Dec. Mean, Tg CH ₄ /yr	A Priori Estimates Annual Mean, Tg CH ₄ /yr	A Posteriori (S1) 1999 Annual Mean, Tg CH ₄ /yr
t7.3	<i>Northern Extratropics</i>			
t7.4 ¹³ C isotopic signature	−53.7‰	−56.2‰	−53.0‰	−51.8‰
t7.5 Bacterial sources, Tg CH ₄ /yr	181	162–197	148	99–134
t7.6 Biomass burning, Tg CH ₄ /yr	2	−46–−18	2	−25–3
t7.8	<i>Tropics</i>			
t7.9 ¹³ C isotopic signature	−50.6‰	−50.2‰	−50.2‰	−50.6‰
t7.10 Bacterial sources, Tg CH ₄ /yr	137	193–195	122	178–181
t7.11 Biomass burning, Tg CH ₄ /yr	52	68–71	48	64–66
t7.13	<i>Southern Extratropics</i>			
t7.14 ¹³ C isotopic signature	−55.8‰	−52.3‰	−56.0‰	−55.1‰
t7.15 Bacterial sources, Tg CH ₄ /yr	52	70–72	48	80–82
t7.16 Biomass burning, Tg CH ₄ /yr	3	17–19	2	11–13

t7.17 ^aNote that the a priori source estimates do not include interannual variability. The differing a priori sources from 1998 to 1999 reflect the seasonality of the sources since the two time-averaged values include different months.

571 the poor observational coverage in these regions, these
572 results must be interpreted with caution. The largest varia-
573 tions in the tropics and southern extratropics over this time
574 period were a moderate decrease in CH₄ flux from tropical
575 South America between 1998 and 1999 and a smaller
576 increase in temperate South America. However, owing to
577 the limited observational constraints on these regions, the
578 partitioning between these regions may not be robust. Since
579 the a posteriori tropical isotopic source signature changes
580 very little from 1998 to 1999, the elevated South American
581 flux estimates in 1998 would most likely be due to an
582 increase in both biomass burning and wetland sources
583 (Table 7). Conversely, in the southern extratropics, while
584 there is little change in the CH₄ flux estimates, the isotopic
585 signatures suggest that there may have been a small
586 increase in bacterial sources and a decrease in biomass
587 burning in 1999.

588 6. Sensitivity of the Results

589 [32] The inverse model was tested for sensitivity to
590 changes in the model, as summarized in Table 3. The first
591 scenario, S0, is simply the a priori CH₄ budget, and S1 is
592 the standard inverse model scenario. If not otherwise
593 specified, discussion of the a posteriori results in this paper
594 refers to S1. S2 applies a more recent measurement of the
595 OH Kinetic Isotope Effect (KIE) [Saueressig *et al.*, 2001].
596 S3 and S4 test the upper and lower limits of the magnitude
597 of the OH sink, based on the uncertainty estimates of
598 Spivakovsky *et al.* [2000]. Finally, in S5 the model
599 sensitivity to initial conditions is tested by initializing the
600 inverse model to hemispheric mean CH₄ mixing ratios and
601 $\delta^{13}\text{C}_{\text{CH}_4}$, rather than the model simulated three-dimensional
602 CH₄ and $\delta^{13}\text{C}_{\text{CH}_4}$ fields used in S1 through S4. The inverse
603 estimates for these scenarios are shown in Tables 4 and 5.

604 [33] In general, the results for the 11 regions CH₄ inver-
605 sion show very little variation between inverse scenarios.
606 Changing the KIE (S2) perturbs the CH₄ estimates very
607 slightly in comparison to S1, the base scenario. This
608 perturbation is due to the iterative process that allows the
609 inverse estimate of the isotopic signature to add constraints
610 to the initial CH₄ inversion. As expected due to the
611 relatively small effect of including this iterative process
612 on the CH₄ inversion, the CH₄ flux estimates are relatively
613 insensitive to this change.

614 [34] Using the upper and lower bounds of the OH fields
615 based on their estimated uncertainty [Spivakovsky *et al.*,
616 2000] in S3 and S4 has a much greater impact on the
617 resulting CH₄ estimates. Changes in the estimated CH₄ flux
618 with changes in the OH field are less than or close to the
619 error estimates for the northern extratropical regions. In the
620 tropical regions of South America, Northern Africa, and
621 Asia, the effect of changes to the OH field is much greater
622 due to the larger concentration of OH in the tropics. The
623 difference between the base scenario and the lower limit of
624 the OH uncertainty exceeds the error estimate on the inverse
625 calculations for these regions. The OH fields in S1 have
626 been scaled up from the original OH fields to match the
627 IPCC [2001] estimate for CH₄ uptake, but the uncertainty
628 limit changes to the OH fields were applied to the original

629 values, so the upper and lower limit OH field scenarios are
630 not symmetrical around the base scenario, S1. In the
631 southern extratropical regions of Southern Africa and
632 Australia, the perturbations to the OH field have relatively
633 little impact on the resulting CH₄ flux estimates, which are
634 fairly similar to the a priori estimates. The largest changes
635 occur in temperate South America. In this region, S1
636 estimates a large increase in CH₄ flux relative to the a priori
637 estimate, but in the lower limit of the OH field estimates,
638 this increase is smaller than the uncertainty estimates for the
639 inverse model. Therefore this result may not be robust in the
640 limit of low OH. Finally, changes in the initial conditions
641 have little effect on the CH₄ flux estimates.

642 [35] The a posteriori isotopic signatures for the five
643 inverse scenarios vary by up to 3.4‰, whereas the varia-
644 tions between the a priori and a posteriori isotopic signa-
645 tures (S0 and S1) are between zero and 1.9‰ (Table 5).
646 This implies that qualitative interpretation of these results
647 based on relative changes between a priori and a posteriori
648 estimates should be treated with caution since the variations
649 with change in model parameters are often larger than these
650 differences.

651 [36] One issue of concern about the sensitivity tests for
652 the isotopic signature inversion is that changes in the initial
653 conditions (S5) have a surprisingly large influence on the
654 inverse estimates. Recent work has shown that the isotopic
655 ratio takes much longer to reach steady state than CH₄
656 [Tans, 1997; Lassey *et al.*, 2000]. The initial conditions for
657 S5 assume a uniform mixing ratio and atmospheric $\delta^{13}\text{C}_{\text{CH}_4}$
658 for each hemisphere for all vertical levels based on the
659 observed hemispheric mean at the surface. In this very poor
660 representation of the atmosphere, it is likely that the 3-
661 month spin-up time is not sufficient for surface fluxes to
662 establish vertical and latitudinal gradients that reflect the
663 atmosphere. However, the current initial conditions, which
664 are based on a preliminary inverse run, should be close
665 enough to the real atmosphere to avoid this problem.

666 [37] Despite these variations in the net isotopic signature
667 of the sources, the quantitative source partitioning estimates
668 are fairly robust with respect to these inverse scenarios
669 (Table 5), providing strong conclusions for the tropics and
670 southern extratropics. In the tropics and southern extra-
671 tropics, all of the inverse scenarios call for increases in both
672 the bacterial and biomass burning sources, although in the
673 low OH limit, these increases are fairly small. Owing to
674 the limited contributions from fossil fuels in these regions,
675 the source partitioning approach provides a very good
676 constraint for these regions.

677 [38] Finally, the partitioning of CH₄ sources into source
678 processes using ¹³C has been shown to be sensitive to errors
679 in the observed isotopic signature of the sources [Miller *et al.*,
680 2002]. The effect of moderate errors in the source
681 signatures used to partition the sources is shown by
682 adjusting each of the isotopic signatures used to partition
683 the sources in turn by ± 2 in Table 8. The source partitioning
684 is somewhat sensitive to these fairly small changes in the
685 isotopic signatures used, especially in the case of the
686 bacterial sources errors in the isotopic signature. For
687 example, a 4‰ change in the bacterial isotopic signature
688 results in a shift of 19 Tg CH₄ from bacterial to biomass

t8.1 **Table 8.** Sensitivity of the Partitioning of the Sources Into Source Processes to the Isotopic Signature of Source Processes^a

t8.2	Model Region	S1	$\delta_{ba} - 2\text{‰}$	$\delta_{ba} + 2\text{‰}$	$\delta_{bb} - 2\text{‰}$	$\delta_{bb} + 2\text{‰}$	$\delta_{ff} - 2\text{‰}$	$\delta_{ff} + 2\text{‰}$
t8.3	<i>Northern Extratropics</i>							
t8.4	Bacterial sources	124–159	117–151	131–198	126–160	122–159	115–154	133–165
t8.5	Biomass burning	–33––5	–26–+3	–40––15	–35––6	–31––5	–25–0.1	–42––11
t8.7	<i>Tropics</i>							
t8.8	Bacterial sources	184–187	174–177	195–198	180–183	188–190	183–187	185–188
t8.9	Biomass burning	65–68	75–78	54–57	69–72	62–64	66–69	65–68
t8.11	<i>Southern Extratropics</i>							
t8.12	Bacterial sources	76–78	72–74	81–83	75–77	77–79	76–78	77–79
t8.13	Biomass burning	13–15	17–20	9–11	14–16	13–15	14–16	13–15

^aThe first column shows the a posteriori sources partitioned into bacterial and biomass burning sources using the isotopic signatures shown in Table 1. Subsequent columns illustrate the effect on the source partitioning of reducing or increasing the bacterial isotopic signature (δ_{ba}), the biomass burning isotopic signature (δ_{bb}), or the fossil isotopic signature (δ_{ff}) by 2‰.

689 burning sources in the tropics (Table 8, columns 2 and 3).
690 However, most of the broad qualitative conclusions of this
691 work still apply.

692 [39] In addition to the likely sources of error that have
693 been tested in this section, the transport model chosen is
694 likely to play an important role in the inverse estimates. For
695 example, the preferred source scenario of *Fung et al.* [1991]
696 was selected by the authors in part because forward model
697 simulations matched the observations so well, but forward
698 simulations of these sources using TM3 result in an over-
699 estimate of the interhemispheric gradient [*Mikaloff Fletcher*,
700 2003]. While most inverse studies of CH₄ have used TM3 or
701 TM2, an earlier version [e.g., *Hein et al.*, 1997; *Houweling*
702 *et al.*, 1999], the recent work of *Chen* [2004] used the
703 Model of Atmospheric Transport and Chemistry (MATCH).
704 There are many similarities between the overall conclusions
705 of *Chen* [2004] and this work. Both inverse studies estimate
706 relatively high fluxes from biomass burning and bacterial
707 sources in the tropics, suggest decreases in fossil emissions,
708 and attribute the bulk of the 1998 CH₄ anomaly to wetlands.
709 However, there are important quantitative differences
710 between the inverse flux estimates. These differences
711 cannot be attributed to the transport model alone because
712 there were many other methodological differences between
713 these two studies, including the inverse methodology, the
714 types of data used, and the representation of the sinks.

715 [40] Finally, the inverse methodology may lead to error.
716 The inverse method used in this study also incorporates
717 only 1 month of model transport, and errors in the a
718 posteriori estimates for a given model transport are likely
719 to be propagated to future months. While the CH₄ inversion
720 is expected to be subject to less aggregation error than
721 source process inversions of CH₄ [e.g., *Mikaloff Fletcher et*
722 *al.*, 2004; *Hein et al.*, 1997], the 11 regions chosen here are
723 still relatively large and are expected to introduce some
724 aggregation error. Owing to the larger regions used for the
725 estimates of the isotopic signatures, aggregation error is
726 likely to be more important for these estimates.

727 7. A Posteriori Atmospheric CH₄ Mixing Ratios 728 and $\delta^{13}\text{CH}_4$

729 [41] Finally, the ability of the inverse estimates to
730 reproduce the atmospheric observations of CH₄ and

$\delta^{13}\text{CH}_4$ is tested. As expected, owing to the observa- 731
732 tional constraints to the inverse model, the a posteriori
733 CH₄ mixing ratio and atmospheric $\delta^{13}\text{CH}_4$ are a far
734 better match to the atmospheric observations than the
735 forward simulation of a priori sources (Figures 1, 5,
736 and 6). The inverse estimates reproduce the observed
737 latitudinal gradient of atmospheric CH₄ very well, cor-
738 recting the overestimate of this gradient that results from
739 the a priori sources (Figure 1, top). The two stations that
740 have unusually high CH₄ mixing ratios for their latitude,
741 Black Sea, Romania, and Cape Rama, India, are not
742 well matched by the inverse estimates due to the strong
743 local source signal for these stations and the higher
744 uncertainty weighting of stations sampling continental
745 air, as discussed by *Mikaloff Fletcher et al.* [2004].
746 The inverse estimates also match the latitudinal gradient
747 of the $\delta^{13}\text{CH}_4$ observations very well, with the model
748 falling within the standard deviation of the observations,
749 based on the standard deviation of the individual observa-
750 tions from the mean, for all of the stations (Figure 1,
751 bottom).

752 [42] In general, monthly mean inverse model results at
753 the observing stations are also in good agreement with the
754 observations for both CH₄ and $\delta^{13}\text{CH}_4$. The observed
755 atmospheric CH₄ mixing ratios and $\delta^{13}\text{CH}_4$ are compared
756 with the simulated CH₄ mixing ratios and $\delta^{13}\text{CH}_4$ based
757 on the a priori and a posteriori estimates (Figures 5 and 6)
758 for the sampling sites with observations of both quantities,
759 described in Table 8. While the a posteriori $\delta^{13}\text{CH}_4$ is
760 generally in good agreement with the observations, it does
761 not capture the full seasonal variability at BRW or the SPO
762 trough in early 1999. In the case of BRW, this may be due
763 to the fact that this site is strongly influenced by CH₄
764 fluxes from boreal North America and Eurasia, which are
765 expected to have a larger relative contribution of wetland
766 CH₄ than the other regions included in the Northern
767 Extratropical latitude band. Therefore the a posteriori
768 isotopic signature which was estimated for an aggregate
769 of all of the northern extratropical regions may not
770 effectively represent conditions at this station. Owing to
771 the dearth of CH₄ sources at high latitudes, the winter
772 trough at SPO is also not well matched by the a posteriori
773 inverse estimates. This anomalous feature may be due to
774 long-term transport of anomalously high wetland emis-

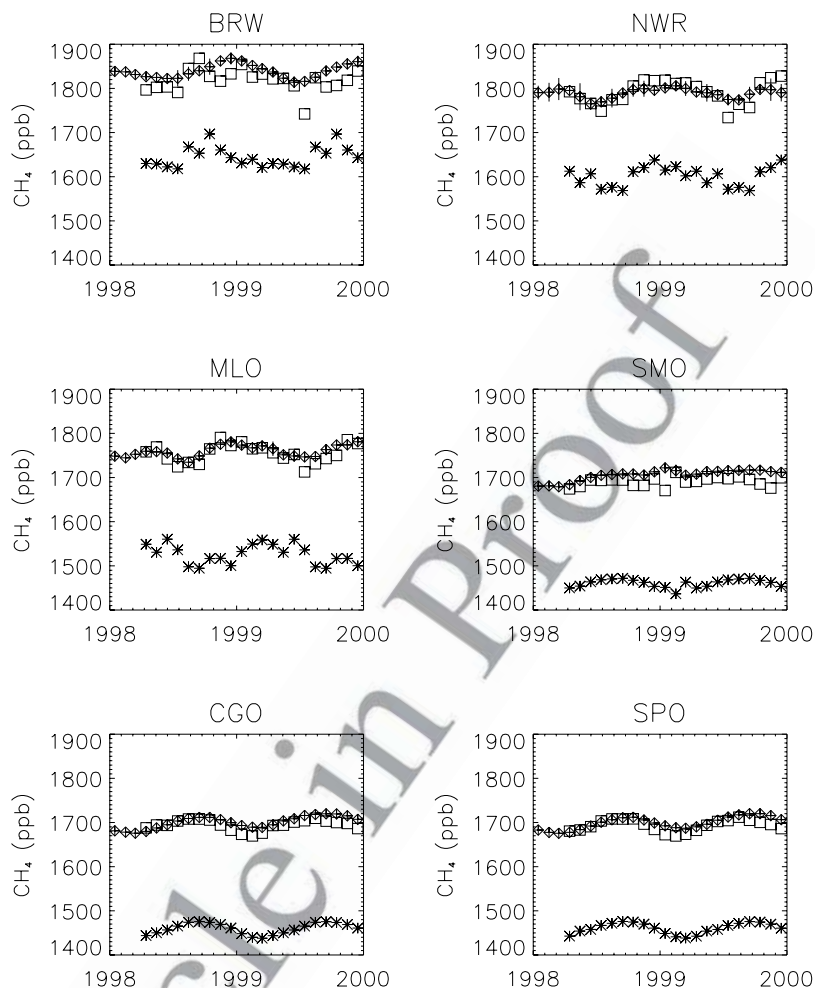


Figure 5. Comparison between the monthly mean CH₄ measurement record at six observing stations (diamonds), model simulation based on a priori sources (asterisks), and the model simulation based on the a posteriori sources (squares). The observing stations are shown in Table 2. Error bars on the measurements represent the standard deviation of the individual observations from the smoothed curve.

775 sions at high southern latitudes at the end of 1998
776 (J. White, personal communication, 2002).

777 [43] The a posteriori atmospheric $\delta^{13}\text{CH}_4$ has also been
778 compared with National Institute of Water and Atmospheric
779 Research (NIWA) observations of $\delta^{13}\text{CH}_4$ at Baring Head,
780 New Zealand, and Scott Base, Antarctica [Lowe *et al.*,
781 1994], which were not used to constrain the inverse model
782 (Figure 7). The modeled $\delta^{13}\text{CH}_4$ is slightly isotopically
783 lighter than the observed values at the NIWA stations, while
784 matching the observations at the CMDL stations. Miller *et al.*
785 [2002] suggested that the NIWA observations might be
786 about 0.1‰ lighter than the CMDL databased on
787 comparisons between observations at Cape Grim and
788 Baring Head, since these two stations are at similar
789 latitudes. However, Figure 7 implies that a source
790 distribution which matches the observations of CH₄ could
791 account for this offset or even a small offset in the opposite
792 direction. Without careful measurement intercomparisons,
793 it is not clear whether the offsets shown in Figure 7 are due

to errors in the inverse estimates or offsets between 794
networks. 795

8. Conclusions 796

[44] A novel, iterative inverse approach was presented 797
estimating the geographical distribution of CH₄ flux and the 798
 $\delta^{13}\text{CH}_4$ isotopic signature of the CH₄ flux that is optimally 799
consistent with the observed spatiotemporal atmospheric 800
CH₄ and $\delta^{13}\text{CH}_4$ distributions. Relative to most bottom-up 801
source estimates, the atmospheric observation call for a large 802
decrease in the NH CH₄ source estimate, a large increase in 803
CH₄ sources in the tropics, and a smaller increase in CH₄ 804
flux from the southern extratropics. This result is robust and 805
in excellent agreement with previous inverse modeling 806
studies of CH₄ [e.g., Hein *et al.*, 1997; Houweling *et al.*, 807
1999; Chen, 2004; Mikaloff Fletcher *et al.*, 2004]. The 808
inverse model yields reduction in the uncertainty of the a 809
priori estimates, especially in NH regions. 810

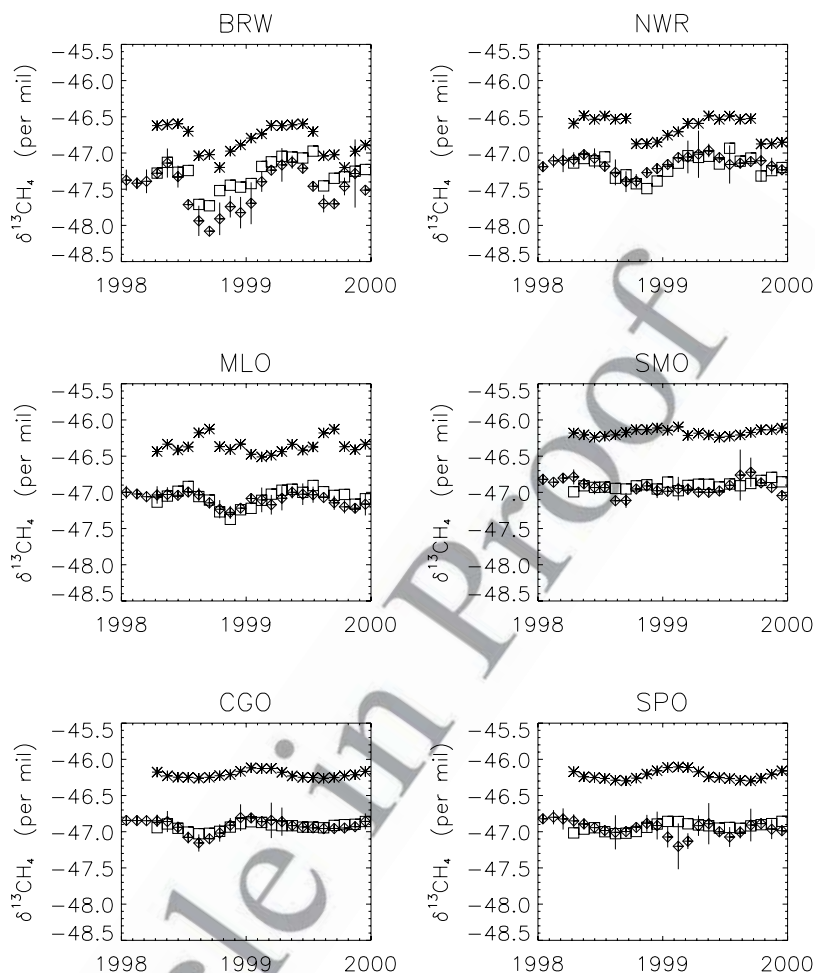


Figure 6. Comparison between the monthly mean $\delta^{13}\text{CH}_4$ measurement record at six observing stations (diamonds), model simulation based on a priori sources (asterisks), and the model simulation based on the a posteriori sources (squares). Error bars on the measurements represent the standard deviation of the individual observations from the smoothed curve.

811 [45] The a posteriori CH_4 fluxes were partitioned into
 812 bacterial and biomass burning sources using inverse esti-
 813 mates of the net isotopic signature of the flux and upper and
 814 lower bound estimates of the fossil fuel and landfill fluxes.
 815 This partitioning technique implies that the estimates for
 816 fossil fuels in the northern extratropics may be inconsistent
 817 with atmospheric observations of CH_4 and $\delta^{13}\text{CH}_4$. In the
 818 tropics and southern extratropics, the source increase in
 819 total CH_4 flux relative to the a priori estimates was
 820 attributed to a large increase in both biomass burning and
 821 swamps.

822 [46] The time-dependent inverse estimates of the CH_4
 823 flux and its isotopic ratios provide new insight into the
 824 causes behind the 1998 growth rate anomaly. The varia-
 825 tions between 1998 and 1999 support the hypothesis of
 826 *Dlugokencky et al.* [2001] that wetlands were primarily
 827 responsible for the anomalous growth rate in 1998, although
 828 increases in biomass burning are also estimated for 1998
 829 over 1999.

830 [47] The total CH_4 flux estimate and the partitioning of
 831 the source between bacterial and biomass burning sources

was generally robust with respect to variations in the KIE 832
 oxidation of CH_4 by OH, the upper bound of the OH 833
 fields, the choice of transport year, and model initializa- 834
 tion. However, the source partitioning was somewhat 835
 sensitive to modest changes in the isotopic signatures of 836
 the sources. 837

[48] The overall agreement in the major conclusions of 838
 this inverse approach and an earlier source-process inver- 839
 sion [*Mikaloff Fletcher et al.*, 2004] suggests that these 840
 results are robust with respect to the model region selection 841
 and the methodology used to incorporate constraints from 842
 the $\delta^{13}\text{CH}_4$. However, there are several significant ongoing 843
 limitations to these inverse estimates. Since this inverse 844
 technique only carries 1 month of model transport at a time, 845
 the monthly variations in the inverse estimates are “noisy” 846
 and the potential to draw robust conclusions from the time 847
 series is limited. Owing to the nonlinearity of the problem, 848
 any errors associated with the CH_4 flux estimates will be 849
 propagated to the estimates of the isotopic signatures. In 850
 addition, error in model transport could introduce signifi- 851
 cant uncertainties. Finally, even with the addition of isotopic 852

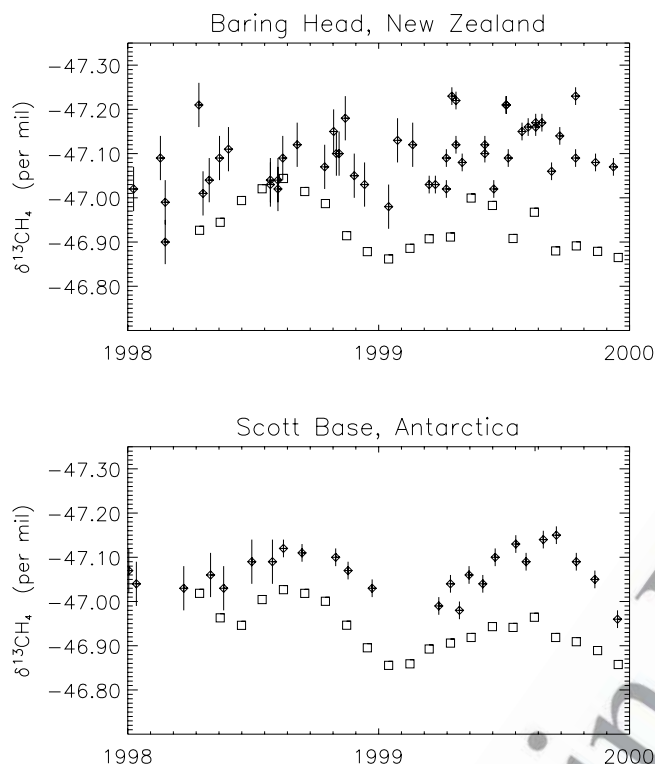


Figure 7. Comparison between the $\delta^{13}\text{CH}_4$ measurement (diamonds) and the model simulation based on the a posteriori sources (squares) for two NIWA observing stations: Baring Head, New Zealand and Scott Base, Antarctica [Lowe et al., 1994].

853 observations, the inverse calculation remains data limited
854 and expansions to the observing network are needed as well.

855 [49] **Acknowledgments.** This paper has benefited greatly from
856 thoughtful discussions and comments from Ed Dlugokencky, Jim White,
857 and Scott Denning. We would like to thank the scientists responsible for
858 the observations that made this work possible, including all of the contribu-
859 tors to the Cooperative Air Sampling Network and the Carbon Cycle
860 Greenhouse Gases Group at NOAA. We are especially grateful to Ed
861 Dlugokencky for his work on methane measurements and interpretation of
862 trends in methane observations, Jim White and INSTARR for the measure-
863 ments of $^{13}\text{C}/^{12}\text{C}$ isotopic ratios in CH_4 , and Ken Masarie for his work on
864 the GLOBALVIEW data product. The authors also acknowledge Dave
865 Lowe, Gordon Brailsford, and Ross Martin for the $\delta^{13}\text{CH}_4$ observations at
866 Baring Head, New Zealand, and Scott Base, Antarctica. S. F., P. T., L. B.,
867 and J. M. acknowledge the NOAA Office of Oceanic and Atmospheric
868 Research for support. S. F. also acknowledges CIRES for support through
869 the Graduate Research Fellowship program and the Biosphere Atmosphere
870 Stable Isotope Network (BASIN) for travel funding that facilitated the
871 development of this work. This research has also been presented in S. F.'s
872 doctoral dissertation at the University of Colorado, Boulder, Boulder,
873 Colorado, USA, 2003.

874 References

875 Aselmann, I., and P. J. Crutzen (1989), Global distribution of natural fresh-
876 water wetlands and rice paddies, their net primary productivity, season-
877 ality, and possible methane emissions, *J. Atmos. Chem.*, **8**, 307–358.
878 Bell, G. D., M. S. Halpert, C. F. Ropelewski, V. E. Kousky, A. V. Douglas,
879 R. C. Schnell, and M. E. Gelman (1999), Climate assessment for 1998,
880 *Bull. Am. Meteorol. Soc.*, **80**, S1–S48.
881 Bergamaschi, P., M. Bräunlich, T. Marik, and C. A. M. Brenninkmeijer
882 (2000), Measurements of the carbon and hydrogen isotopes of atmo-

spheric methane at Izaña, Tenerife: Seasonal cycles and synoptic-scale 883
variations, *J. Geophys. Res.*, **105**, 14,531–14,546. 884
Bingemer, H. G., and P. J. Crutzen (1987), The production of methane from 885
solid wastes, *J. Geophys. Res.*, **92**, 2181–2187. 886
Brenninkmeijer, C. A. M., D. C. Lowe, M. R. Manning, R. J. Sparks, and 887
P. F. J. van Velthoven (1995), The ^{13}C , ^{14}C , and ^{18}O isotopic composition 888
of CO , CH_4 , and CO_2 in the higher southern latitudes lower stratosphere, 889
J. Geophys. Res., **100**, 26,163–26,172. 890
Bruhwiler, L., P. Tans, and M. Ramonet (2000), A time-dependent assimila- 891
tion and source retrieval technique for atmospheric tracers, in *Inverse* 892
Methods in Global Biogeochemical Cycles, *Geophys. Monogr. Ser.*, 893
vol. 114, edited by P. Kasibhatla et al., pp. 265–277, AGU, Washington, 894
D. C. 895
Cantrell, C. A., R. E. Shetter, A. H. McDaniel, J. G. Calvert, J. A. Davidson, 896
D. C. Lowe, S. C. Tyler, R. J. Cicerone, and J. P. Greenberg (1990), 897
Carbon kinetic isotope effect in the oxidation of methane by the hydroxyl 898
radical, *J. Geophys. Res.*, **95**, 22,455–22,462. 899
Chen, Y.-H. (2004), Estimation of methane and carbon dioxide surface 900
fluxes using a 3-D global atmospheric chemical transport model, Ph.D. 901
thesis, Mass. Inst. of Technol., Cambridge, Mass. 902
Cicerone, R. J., and R. S. Oremland (1988), Biogeochemical aspects of 903
atmospheric methane, *Global Biogeochem. Cycles*, **2**, 299–327. 904
Craig, H. (1953), The geochemistry of stable carbon isotopes, *Geochim.* 905
Cosmochim. Acta, **3**, 53–92. 906
Curtis, S., R. Adler, G. Huffman, E. Nelkin, and D. Bolvin (2001), Evolu- 907
tion of tropical and extratropical precipitation anomalies during the 908
1997–1999 ENSO Cycle, *Int. J. Climatol.*, **21**, 961–967. 909
Dlugokencky, E. J., B. P. Walter, K. A. Masarie, P. M. Lang, and E. S. 910
Kasische (2001), Measurements of an anomalous global methane 911
increase during 1998, *Geophys. Res. Lett.*, **28**, 499–502. 912
Dlugokencky, E. J., S. Houweling, L. Bruhwiler, K. A. Masarie, P. M. 913
Lang, J. B. Miller, and P. P. Tans (2003), Atmospheric methane levels 914
off: Temporary pause or a new steady state?, *Geophys. Res. Lett.*, **30**(19), 915
1992, doi:10.29/2003GL017475. 916
Fraser, I., J. John, J. Lerner, E. Matthews, M. Prather, L. P. Steele, and P. J. 917
Fraser (1991), Three-dimensional model synthesis of the global methane 918
cycle, *J. Geophys. Res.*, **96**, 13,033–13,065. 919
Heimann, M., and S. Körner (2003), The Global Atmospheric Tracer Model 920
TM3 model description and user's manual, technical report, Max-Planck- 921
Inst. für Biogeochem., Jena, Germany. 922
Hein, R., P. J. Crutzen, and M. Heimann (1997), An inverse modeling 923
approach to investigate the global atmospheric methane cycle, *Global* 924
Biogeochem. Cycles, **11**, 43–76. 925
Houweling, S., T. Kaminski, F. Dentener, J. Lelieveld, and M. Heimann 926
(1999), Inverse modeling of methane sources and sinks using the ad- 927
joint of a global transport model, *J. Geophys. Res.*, **104**, 26,137– 928
26,160. 929
Intergovernmental Panel on Climate Change (2001), *Climate Change 2001:* 930
The Scientific Basis, edited by J. T. Houghton et al., Cambridge Univ. 931
Press, New York. 932
Kaminski, T., M. Heimann, and R. Giering (1999), A coarse grid three- 933
dimensional inverse model of the atmospheric transport: 1. Adjoint model 934
and Jacobian matrix, *J. Geophys. Res.*, **104**, 18,535–18,553. 935
Kaplan, J. O. (2001), Wetlands at the Last Glacial Maximum: Distribution 936
and methane emissions, *Geophys. Res. Lett.*, **29**, 6–10. 937
Lassey, K. R., D. C. Lowe, and M. R. Manning (2000), The trend in 938
atmospheric methane $\delta^{13}\text{C}$ and implications for isotopic constraints on 939
the global methane budget, *Global Biogeochem. Cycles*, **14**, 41–49. 940
Lelieveld, J., P. J. Crutzen, and F. S. Dentener (1998), Changing concentra- 941
tion, lifetime, and climate forcing of atmospheric methane, *Tellus, Ser.* 942
B, **50**, 128–150. 943
Levine, J. S., W. R. Coffey III, and J. P. Pinto (2000), Biomass burning, in 944
Atmospheric Methane: Its Role in Global Environment, edited by M. A. 945
K. Khalil, Springer-Verlag, New York. 946
Lowe, D. C., C. A. M. Brenninkmeijer, G. W. Brailsford, K. Lassey, A. J. 947
Gomez, and E. G. Nisbet (1994), Concentration and ^{13}C records of atmo- 948
spheric methane in New Zealand and Antarctica: Evidence for changes in 949
methane sources, *J. Geophys. Res.*, **99**, 16,913–16,925. 950
Matthews, E., and I. Fung (1987), Methane emissions from natural wet- 951
lands: Global distribution, area, and environmental characteristics of 952
sources, *Global Biogeochem. Cycles*, **1**, 61–86. 953
Mikaloff Fletcher, S. E. M. (2003), Constraining methane flux estimates 954
using observations of atmospheric methane and $^{13}\text{C}/^{12}\text{C}$ isotopic ratios in 955
methane, Ph.D. thesis, Univ. of Colo., Boulder. 956
Mikaloff Fletcher, S. E., P. P. Tans, L. M. Bruhwiler, J. B. Miller, and 957
M. Heimann (2004), CH_4 sources estimated from atmospheric observa- 958
tions of CH_4 and its $^{13}\text{C}/^{12}\text{C}$ isotopic ratios: 1. Inverse modeling of source 959
processes constraining CH_4 source estimates with atmospheric observa- 960

- 961 tions of CH₄ and ¹³C/¹²C isotopic ratios in CH₄ in an inverse model,
 962 *Global Biogeochem. Cycles*, doi:10.1029/2004GB002223, in press.
- 963 Miller, J. B., K. A. Mack, R. Dissly, J. W. C. White, E. J. Dlugokencky, and
 964 P. P. Tans (2002), Development of analytical methods and measurements
 965 of ¹³C/¹²C in atmospheric CH₄ from the NOAA/CMDL global air sam-
 966 pling network, *J. Geophys. Res.*, 107(D13), 4178, doi:10.1029/
 967 2001JD000630.
- 968 National Oceanic and Atmospheric Administration, (2001), GLOBALVIEW-
 969 CH₄: Cooperative Atmospheric Data Integration Project- Methane
 970 [CD-ROM], report, Clim. Monit. and Diag. Lab., Boulder, Colo. (Also
 971 available at ftp.cmdl.noaa.gov, Path: ccg/ch4/GLOBALVIEW)
- 972 Olivier, J. G. J., A. F. Bouwman, C. W. M. van der Maas, J. M. Berdowski,
 973 C. Veldt, J. P. J. Bloos, A. J. H. Visschedijk, P. J. Zandveld, and J. L.
 974 Haverlag (1996), Description of Edgar Version 2.0: A set of global emis-
 975 sion inventories of greenhouse gases and ozone-depleting substances for
 976 all anthropogenic and most natural sources on a per country basis and on
 977 1 × 1 grid, report, Natl. Inst. of Public Health and the Environ., Biltho-
 978 ven, Netherlands.
- 979 Petit, J. R., et al. (1999), Climate and atmospheric history of the past 42,000
 980 years from the Vostok ice core, Antarctica, *Nature*, 399, 429–436.
- 981 Quay, P., J. Stutsman, D. Wilbur, A. Snover, E. Dlugokencky, and T. Brown
 982 (1999), The isotopic composition of atmospheric methane, *Global Bio-
 983 geochem. Cycles*, 13, 445–461.
- 984 Sanderson, M. G. (1996), Biomass of termites and their emissions of
 985 methane and carbon dioxide: A global database, *Global Biogeochem.
 986 Cycles*, 10, 543–557.
- 987 Saueressig, G., J. N. Crowley, P. Bergamaschi, C. Brühl, C. A. M.
 988 Brenninkmeijer, and H. Fischer (2001), Carbon 13 and D kinetic iso-
 989 tope effects in the reactions of CH₄ with O (¹D) and OH: New labora-
 990 tory measurements and their implications for the isotopic composition
 991 of stratospheric methane, *J. Geophys. Res.*, 106, 23,127–23,138.
- Spivakovsky, C. M., et al. (2000), Three-dimensional climatological dis- 992
 tribution of tropospheric OH: Update and evaluation, *J. Geophys. Res.*, 993
 105, 8931–8980. 994
- Tans, P. P. (1997), A note on isotopic ratios and the global atmospheric 995
 methane budget, *Global Biogeochem. Cycles*, 11, 77–81. 996
- Tyler, S. C., P. M. Crill, and G. W. Brailsford (1994), ¹³C/¹²C fractionation 997
 of methane during oxidation in a temperate forested soil, *Geochim.* 998
Cosmochim. Acta, 58, 1625–1633. 999
- Walter, B. (1998), Development of a process-based model to derive 1000
 methane emissions from natural wetlands for climate studies, Ph.D. 1001
 thesis, Univ. Hamburg, Germany. 1002
- Warwick, N. J., S. Bekki, K. S. Law, E. G. Nisbet, and J. A. Pyle (2002), 1003
 The impact of meteorology on the interannual growth rate of atmospheric 1004
 methane, *Geophys. Res. Lett.*, 29, 1947–1951. 1005
- Whiticar, M. (1993), Stable isotopes in global budgets, in *Atmospheric* 1006
Methane—Sources, Sinks, and Role in Environmental Change, NATO 1007
ASI Ser.: Global Environ. Change, vol. 1, edited by M. A. K. Khalil, 1008
 Springer-Verlag, New York. 1009
- L. Bruhwiler, J. Miller, and P. Tans, NOAA CMDL, R/CMDL-1, 325 1011
 Broadway, Boulder, CO 80305, USA. (lori.bruhwiler@noaa.gov; john.b. 1012
 miller@cmdl.noaa.gov; pieter.tans@noaa.gov) 1013
- M. Heimann, Max-Planck-Institut für Biogeochemie, Postfach 10064, 1014
 D-0771 Jena, Germany. (martin.heimann@bgc-jena.mpg.de) 1015
- S. Mikaloff Fletcher, Department of Atmospheric and Oceanic Sciences, 1016
 University of California, Los Angeles, 5839 Schlichter Hall, Los Angeles, 1017
 CA 90024, USA. (fletcher@igpp.ucla.edu) 1018
 1019